Nanoscale

Check for updates

Low-frequency electronic noise in superlattice and random-packed thin films of colloidal quantum dots†

Adane Geremew, [ID] [a] Caroline Qian,[b] Alex Abelson,[c] Sergey Rumyantsev, [ID] [a,d] Fariborz Kargar, [ID] [a] Matt Law[b,c,e] and Alexander A. Balandin [ID] *[a,f]

We report measurements of low-frequency electronic noise in ordered superlattice, weakly-ordered and random-packed thin films of 6.5 nm PbSe quantum dots prepared using several different ligand chemistries. For all samples, the normalized noise spectral density of the dark current revealed a Lorentzian component, reminiscent of the generation–recombination noise, superimposed on the $1/f$ background (f is the frequency). An activation energy of ~0.3 eV was extracted from the temperature dependence of the noise spectra in the ordered and random quantum dot films. The noise level in the ordered films was lower than that in the weakly-ordered and random-packed films. A large variation in the magnitude of the noise spectral density was also observed in samples with different ligand treatments. The obtained results are important for application of colloidal quantum dot films in photodetectors.

[a]*Nano-Device Laboratory (NDL), Department of Electrical and Computer Engineering, University of California, Riverside, California 92521, USA. E-mail: balandin@ece.ucr.edu; https://balandingroup.ucr.edu/*
[b]*Department of Chemical and Biomolecular Engineering, University of California, Irvine, California 92697, USA*
[c]*Department of Materials Science and Engineering, University of California, Irvine, California 92697, USA*
[d]*CENTERA Laboratories, Institute of High-Pressure Physics, Polish Academy of Sciences, Warsaw 01-142, Poland*
[e]*Department of Chemistry, University of California, Irvine, California 92697, USA*
[f]*Phonon Optimized Engineered Materials (POEM) Center, Materials Science and Engineering Program, University of California, Riverside, California 92521, USA*
†Electronic supplementary information (ESI) available. See DOI: 10.1039/c9nr06899f

Solution-processed quantum dot (QD) optoelectronic devices may offer low cost, large area, mechanically flexible and manufacturable large-scale device integration.[1–5] Solution-based processes include spin coating, dip coating, Langmuir-Schaefer deposition, spraying and inkjet printing. Typically, the performance of solution-processed devices is inferior to the performance of devices fabricated by conventional techniques. However, the low cost, scalability and other benefits make solution-processed optoelectronics attractive for a range of applications, including photodetectors, light emitting diodes and solar cells.[5–12] Colloidal QDs can be used to prepare random-packed or ordered QD thin films. Spatially-ordered QD assemblies are often called quantum dot superlattices (QD SLs).[1] The optical and electronic properties of QD SLs depend not only on the intrinsic characteristics of QDs but also on the QD packing density, orientation, inter-QD distance and dielectric medium. Tunable electronic band structures make QD SLs attractive for detector and photovoltaic applications.[5,13,14] The low thermal conductivity of QD films also suggests applications in thermoelectrics.[1,15]

It is predicted theoretically that QD SLs with small QD size and inter-dot distance and low levels of defects and disorder offer attractive possibilities for controlling the electronic band structure and acoustic phonon dispersion.[14,16] Strong electron wave function overlap in QD SLs can lead to formation of electronic mini-bands, and, as a result, substantially higher charge carrier mobility than is achievable in films of otherwise-comparable random-packed QDs. The long-range order of QDs is essential for formation of mini-bands and emergence of band transport instead of the hopping transport characteristic of random QD films. Long-range order can also lead to strong modification of the acoustic phonon dispersion, with corresponding changes in electron–phonon scattering and light–matter interactions.[12,14–17] For more than two decades, the efforts in synthesis and testing of QD SLs synthesized by molecular beam epitaxy,[18–20] solution processing[21–23] and other techniques[24] were focused on improving the long-range order to achieve formation of coherent mini-bands and, correspondingly, enhanced electron mobility and modified optical response.[1] There have been only a few studies of current fluctuation and noise processes in QD films and devices.[25–28] We are aware of only one detailed report on low-frequency noise in colloidal QD films.[27] Knowledge of the low-frequency noise characteristics of QD films is important from both the

fundamental and applied points of view. Noise characteristics can provide insight into charge transport and tunneling mechanisms in QD films. Understanding of noise mechanisms and development of noise reduction approaches are important for practical applications of QD films in photodetectors.

In this Letter, we report low-frequency noise measurements in three types of QD thin films: highly-ordered, polycrystalline QD superlattices made by Langmuir-Schaefer deposition (LS films), weakly-ordered spin-cast films (SC films), and random-packed dip-coated films (DC films). We find that the LS films have less noise than the SC and DC films. The difference in the noise spectral density between the LS and DC films varies from a factor of two to more than two orders of magnitude at room temperature (RT). The noise levels of DC films with different ligand chemistries, i.e., films prepared with ethylene-diamine versus ammonium thiocyanate, span more than an order of magnitude. One important finding is that the spectra of all films show a Lorentzian component superimposed on the $1/f$ background, reminiscent of generation–recombination (G–R) noise. Interestingly, the same activation energy of ~0.3 eV was extracted from the noise temperature dependence of LS superlattice and DC random QD films, prepared by different chemistries. The obtained results have important implications for proposed applications of QDs in photodetectors because low-frequency noise often limits the detectivity and selectivity of photodetectors and sensors.[29–34] Our observation of lower noise in QD superlattices provides additional motivation for research to improve the long-range order of colloidal QD superlattices.

In this study, we fabricated 30–70 nm thick films of 6.5 nm PbSe QDs using three different methods and ligand chemistries in order to study the impact of spatial order and surface chemistry on low-frequency noise (see Table 1). All films were infilled and overcoated with a 20 nm thick layer of amorphous aluminum oxide via atomic layer deposition (ALD) to prevent oxidation of the QDs.[35] To investigate the role of spatial order, we fabricated epitaxial superlattice (epi-SL) films with ~250 nm lateral SL grain sizes via self-assembly of QDs on a liquid surface (the Langmuir-Schaefer technique).[36,37] These LS films contain a mixture of adsorbed ethylene glycoxide, iodide and residual oleate surface ligands. The second type of

sample (the SC films) feature ~25 nm lateral superlattice grains and similar surface ligands and coverage as the LS films. These films have very similar surface chemistry to the epi-SL films. On a sub-100 nm length scale, the LS superlattice films possess more uniform inter-QD distances and connectivity due to oriented attachment (i.e., epitaxial fusion of the QDs) in three dimensions.[37,38] At a length scale below 10 μm, the SC films are smooth and continuous whereas the LS films have more significant macroscopic cracking that occurs during QD self-assembly. Scanning electron microscope (SEM) images highlighting these differences are provided in Fig. 1. The third type of sample was random-packed QD films prepared by dip coating (DC films) using either ethylenediamine (DC EDA) or ammonium thiocyanate (DC SCN #1 and #2) ligand treatments. These films were deposited using a layer-by-layer dip coating process that yields optically smooth, continuous, and dense films (see Fig. 1).[39] The DC SCN films contain adsorbed thiocyanate and the DC EDA films possess a mixture of oleate and ethylenediamine ligands. Fourier transform infrared (FTIR) spectra shown in the ESI† highlight the differences in surface chemistry between the samples studied here.

For electrical and noise measurements, we prepared QD films on SiO_2/Si wafers pre-patterned with metal contacts. Ti/Au contacts (5 nm/35 nm) were separated by a channel with a length of 25 μm and width of 1000 μm, as defined by conventional photolithography The quantum-confined band gap of the QDs in solution was 0.69 eV, as expected for 6.5 nm PbSe QDs. The bulk band gap of PbSe is 0.29 eV at RT.[40,41] All of the devices showed n-channel behavior after ALD infilling, with an electron mobility in the range of 1–4 $cm^2 V^{-1} s^{-1}$, which is typical for such materials.[1,3] Fig. 2(a) shows a schematic of the fabricated devices. The current–voltage (I–V) characteristics of the devices were measured with a semiconductor parameter analyzer (Agilent B1500). Fig. 2(b) shows the electrical resistivity, ρ, for representative QD films of all three types (LS, SC, and DC) as a function of temperature, T. The sample names in the legend correspond to those in the Table 1. Since the focus of the present study is on the dark current noise characteristics, the data in Fig. 2(b) were measured without illumination.

The resistivity of the LS superlattice films was smaller than that of the SC and DC random QD films (see Fig. 2(b)). For all

Table 1 Characteristics of the colloidal quantum dot thin films

| Samples name	Film type	Ligand treatment	S_I/I^2 (Hz^{-1}) $T = 100$ K $f = 10$ Hz	S_I/I^2 (Hz^{-1}) $T = 300$ K $f = 10$ Hz
DC SCN #1	Dip coated (DC); random-packed QDs	Ammonium thiocyanate (SCN)	5.80×10^{-9}	1.85×10^{-10}
DC SCN #2	Dip coated (DC); random-packed QDs	Ammonium thiocyanate (SCN)	3.98×10^{-6}	4.38×10^{-10}
DC EDA #1	Dip coated (DC); random-packed QDs	Ethylenediamine in acetonitrile	2.31×10^{-9}	2.63×10^{-8}
SC EDA #1	Spin coated (SC); weakly-ordered QDs	Ethylenediamine in ethylene glycol + PbI_2 in dimethylsulfoxide	1.04×10^{-9}	1.42×10^{-8}
LS #1	epi-Superlattice; long-range order	Ethylenediamine in ethylene glycol + PbI_2 in dimethylsulfoxide	5.86×10^{-11}	2.91×10^{-11}
LS #2	epi-Superlattice; long-range order	Ethylenediamine in ethylene glycol + PbI_2 in dimethylsulfoxide	2.43×10^{-10}	6.32×10^{-11}
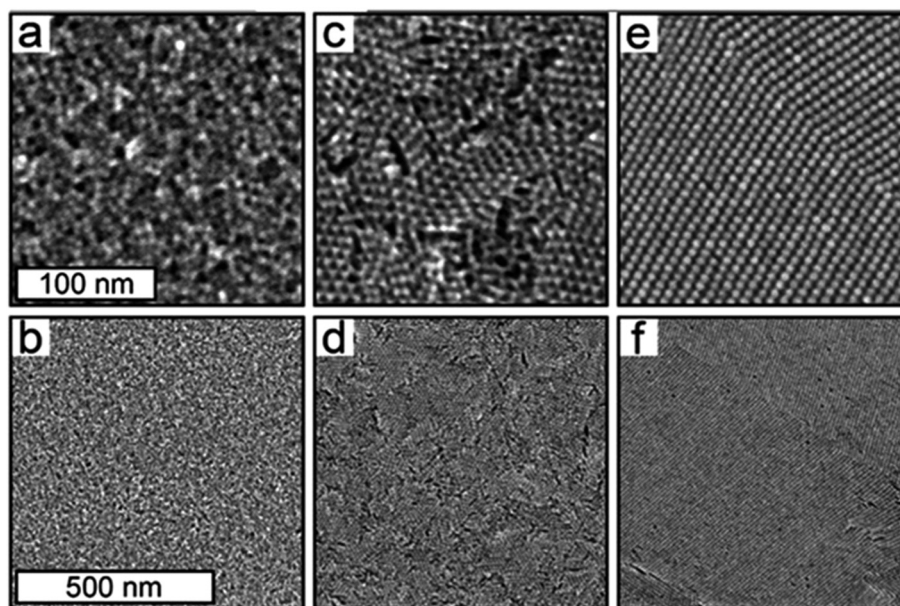
Fig. 1 Scanning electron microscope images of QD films with varying degrees of long-range order. (a–b) Dip-coated films, corresponding to samples "DC SCN #1", "DC SCN #2" and "DC EDA #1" in Table 1. (c–d) Spin-coated films with short-range order, corresponding to sample "SC EDA #1" in Table 1. (e–f) Langmuir-Schaefer *epi*-superlattice films with long-range order, corresponding to samples "LS #1" and "LS #2" in Table 1.

three types of samples, the resistivity decreases with temperature, suggesting that transport occurs by phonon-assisted tunneling, *i.e.*, hopping.[42–45] The hopping conductance is commonly analyzed using the expression[43]

$$G = G_0 e^{-(T_0/T)^p}$$

where T_0 depends on the material properties and the localization length in the given structure and p is a parameter defined by the type of hopping. The resistivity data analysis using Arrhenius plots and the $\ln(G)$ *vs.* $\ln(T)$ dependence (see ESI†) indicate nearest-neighbor hopping (NNH) in the high-temperature region and variable-range hopping (VRH) at lower temperature. Similar temperature dependences of the conductivity for PbSe QDs of the same diameter were reported in ref. 37. From the Arrhenius plot, we extracted activation energies of 0.171 eV and 0.137 eV for NNH transport in the DC and LS films, respectively.

The noise spectra were determined with a dynamic signal analyzer (Stanford Research) with inbuilt low-noise amplifier. The devices were DC biased with a "quiet" battery-potentiometer circuit in order to minimize 60 Hz noise from the electrical grid. The noise measurements were conducted in a two-terminal device configuration. Details of our noise measurement procedures have been reported elsewhere.[46–48] In Fig. 3(a), we present the normalized current noise spectral density, S_I/I^2, as a function of frequency, f, at different temperatures (I is the current through the device) for a representative LS and DC QD film. The measurements were conducted at a source–drain bias of 1.0 V. Fig. 3(b) shows S_I/I^2 as a function of frequency at different bias voltages. In the studied set of

samples, the LS superlattice films produce less noise than the DC random QD films at all bias voltages and temperatures. For some f and T, the difference in the noise level, S_I/I^2, is more than an order of magnitude.

For all samples, we examined the noise spectral density scaling with the current (see Fig. 4(a) and (b)). The noise in all samples followed the $S_I \sim I^2$ trend with only small deviations. This indicates that the electrical current does not induce strong Joule heating, annealing or other structural or morphological changes.[49] This is in contrast to a previous report of low-frequency noise in colloidal QD films, which revealed strong deviation from the $S_I \sim I^2$ dependence.[27] In Fig. 4(c), we present the normalized noise spectral density, S_I/I^2, as a function of temperature. The noise level in the LS films is the lowest of all examined samples. However, at certain temperature and bias ranges, the noise spectral density in LS films becomes rather close to that in the DC films. The difference in the noise level between DC and SC films is also large. For this reason, it is difficult to establish from these data the relative importance of spatial order, ligand chemistry, and other factors determining the noise level in QD films.

As one can see from Fig. 3(a) and 4(c), both the amplitude of noise and shape of the spectra depend on temperature. Similar to G–R noise in semiconductors, which appears as Lorentzian peaks, this can be a result of a random process with a well-defined characteristic time that depends on temperature.[29,50–52] In general, the spectral density of G–R noise is described by the Lorentzian: $S_I(f) = S_0/[1 + (2\pi f\tau)^2]$, where S_0 is the frequency independent portion of $S_I(f)$ observed at $f \ll f_c = (2\pi\tau)^{-1}$ and τ is the time constant associ-
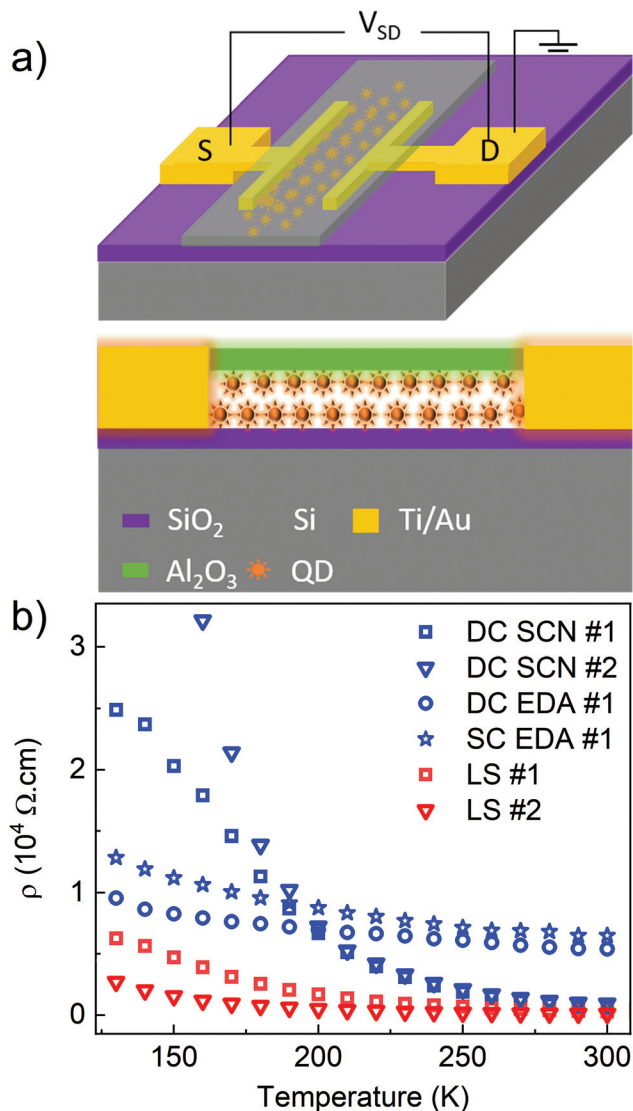
Fig. 2 (a) Schematics of the QD devices showing perspective (top panel) and cross-sectional (bottom panel) views. (b) Electrical resistivity of the LS, SC, and DC films as a function of temperature. The decrease in resistivity with increasing temperature is consistent with hopping transport.

Fig. 3 (a) Normalized current noise spectral density, S_I/I^2, as a function of frequency at different temperatures. The data are presented for two samples: ordered LS #1 (dashed lines) and random DC SCN #1 (solid lines). (b) Normalized current noise spectral density, S_I/I^2, as a function of frequency for different source–drain biases, shown for the same devices as in (a). The noise level in the ordered LS film is consistently lower than that in the random DC films.

ated with the return to equilibrium of the occupancy of the trap level. In typical semiconductors, the spectral density of the G–R noise is often expressed as,[50]

$$\frac{S_I}{I^2} = \frac{4N_t}{Vn^2} \frac{\tau F(1-F)}{1 + (\omega\tau)^2},\tag{1}$$

where $\omega = 2\pi f$, V is the sample volume, n is the equilibrium electron concentration for an n-type material, and F is the trap state occupancy function. The G–R noise time constant, τ, can be further related to the trap state capture and release time constants. The most common description of 1/f noise, dominated by fluctuations in the number of charge carriers, N, stems from the observation that a superposition of individual G–R noise sources with the lifetime distributed on a exponen-
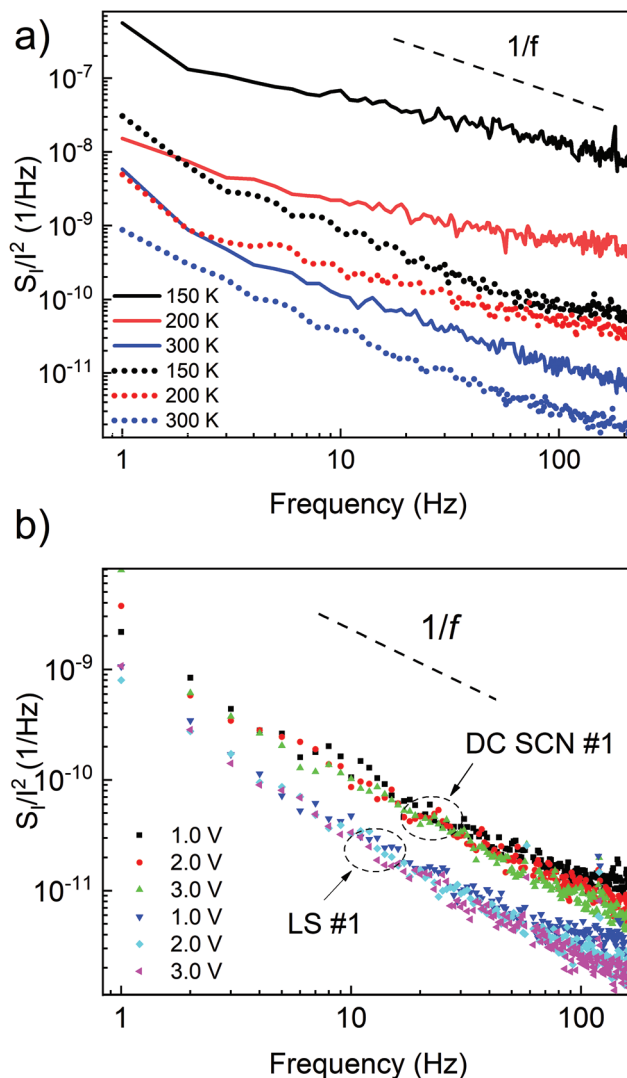
tially wide timescale, within the τ_1 and τ_2 limits, gives the 1/f type spectrum in the intermediate range of frequencies $1/\tau_2 < \omega < 1/\tau_1$. If one specific G–R noise source, *e.g.* trap with the well-defined τ, dominates the noise spectrum owing to its much higher concentration, then the Lorentzian associated with this trap appears superimposed over the 1/f background. Our experimental observation appears to be in line with this mechanism. In order to characterize this kind of process, it is common to plot the normalized noise spectral noise density multiplied by frequency, $S_I/I^2 \times f$, *versus* frequency. The position of the maximum, f_c, of this dependence defines the characteristic time of the random process, $\tau = 1/2\pi f_c$, at a given temperature. If the characteristic time depends exponentially
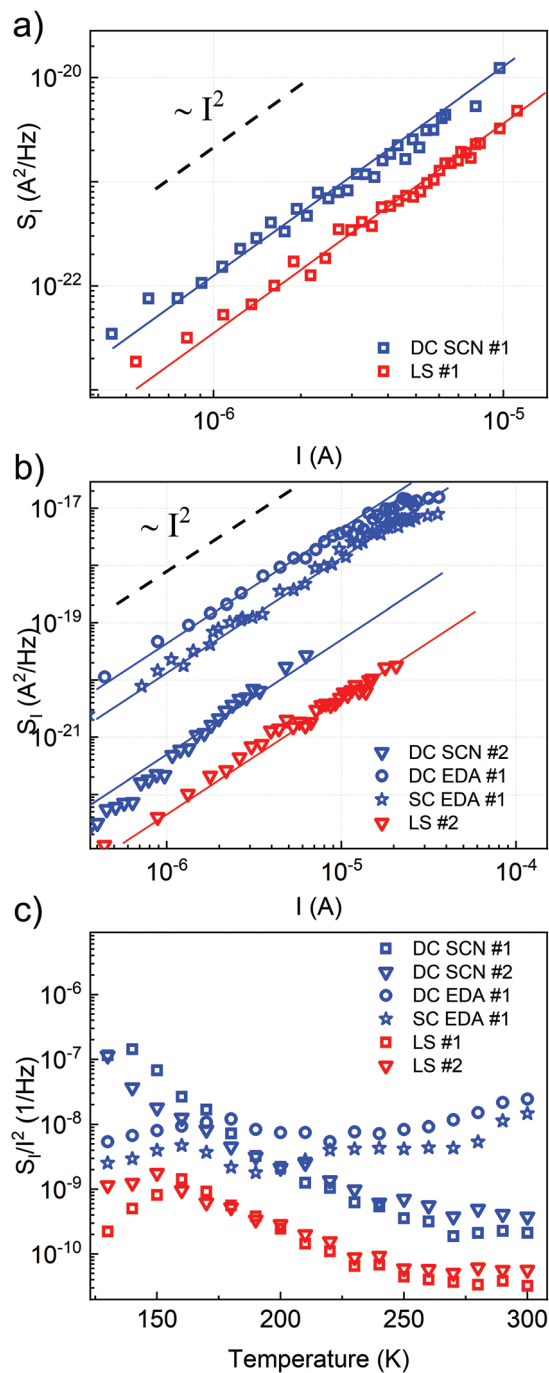
Fig. 4 (a−b) Noise spectral density, S_I, as a function of current, I. The data are presented in two panels to clearly show the difference between the LS and DC films that had relatively close noise levels. Note that the slope is proportional to $\sim I^2$ for all samples. (b) Normalized noise spectral density, S_I/I^2, as a function of temperature, T, for the examined QD films. The noise spectral density was measured at $f = 10$ Hz in both (a) and (b).

From our data, one can see that at low temperatures and low frequencies, the shape of the measured spectra is close to $1/f^2$, indicating the presence of a Lorentzian component with characteristic frequency below 1 Hz, i.e., below the limits of our experimental setup. At high temperatures, the Lorentzian components are barely noticeable because they are masked by the $1/f$ noise. For this reason, we used an alternative approach for finding the characteristic time, τ, by plotting the noise spectral density as a function of temperature at different frequencies.[53,54] If these dependences have maxima, it is assumed that $\tau = 1/2\pi f_c$ at the temperature of the maximum, T_m. The Arrhenius plot of $\ln(f_c)$ versus $1/T_m$ allows one to find the activation energy for the noise process. Fig. 5(a and b) show S_I/I^2 at different frequencies as a function of temperature. The dependences in Fig. 5(a) and (b) have clear maxima shifting with temperature, reflecting the temperature dependence of f_c.

Fig. 6 shows the plot of $\ln(f_c)$ vs. $1/T_m$ that was used to extract the noise activation energies. The activation energy for the LS and DC films is nearly equal at $\sim$0.3 eV. This activation
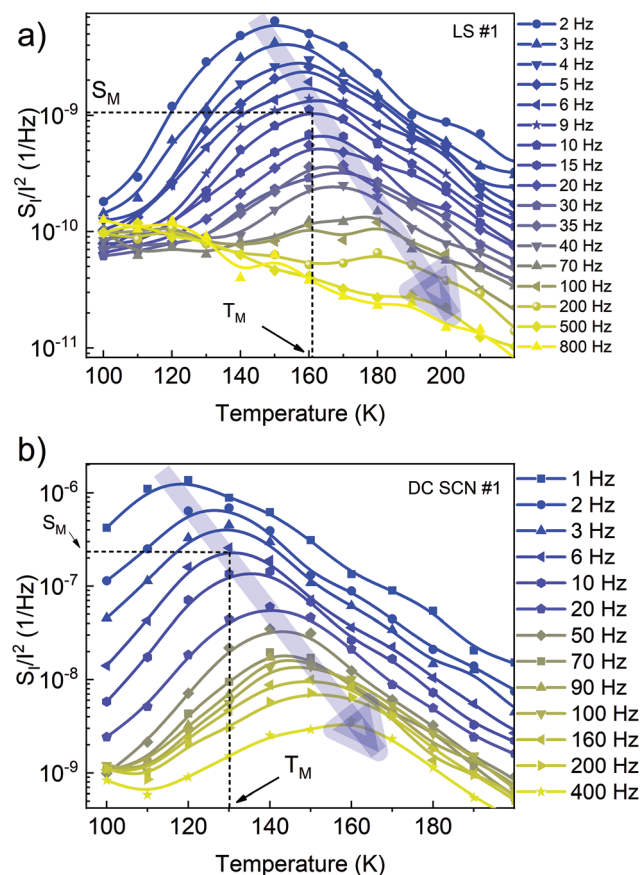

Fig. 5 (a) Normalized current noise spectral density, S_I/I^2, as a function of temperature for different frequencies for the ordered sample LS #1. (b) The same as in (a) for the random sample DC SCN #1. The blue arrows are guides to the eye, indicating the shift in the maximum of the noise spectral density with temperature. The dotted lines illustrate the process of finding the noise maximum for each temperature.
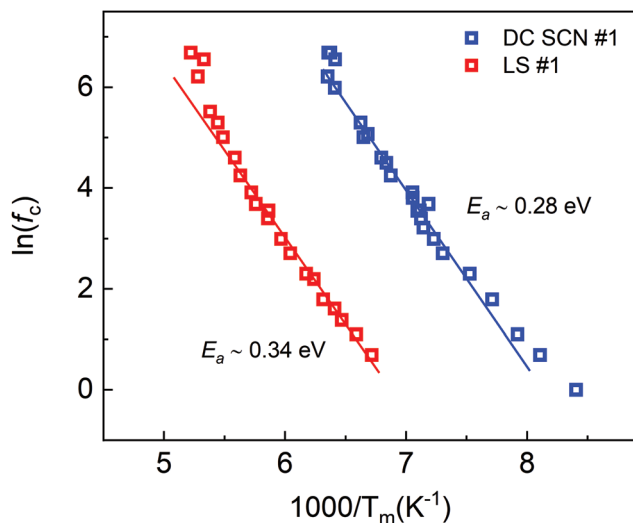
on temperature, an Arrhenius plot allows extraction of the activation energy of this random process. However, such a method is inapplicable if the position of the maximum is outside of the studied frequency range or not clearly observed due to the $1/f$ noise background.

Fig. 6 Arrhenius plot, $\ln(f_c)$ vs. $1/T$, for the samples LS #1 and DC SCN #1. The similarity of the activation energies extracted from the noise spectra suggest the same noise mechanism in different types of QD films.

energy is significantly higher than the activation energy of the NNH conductivities. Therefore, the temperature dependences of the conductivity and noise appear to be regulated by different mechanisms. This is a rather common situation in semiconductors. For example, G–R noise with a strong temperature dependence is often observed even when the conductivity is temperature independent.[43,49,55–57] The LS and DC samples have been fabricated by different methods and have different ligands. The same activation energy of the noise in these devices can be an indication of the same noise mechanism. The energies close to 0.3 eV can be associated with the certain trapping states in QDs, ligands or chemistries used in QD treatment (see ESI†). The variation in the noise level in the ordered and random QD films can also be associated with the number of conducting channels in the QD films, which depend on the inter-dot distance, presence of cracks and variation of the QD density. Under the realistic assumption of independent fluctuators uniformly distributed in the sample, the normalized noise spectral density is inversely proportional to the volume of the conducting channels, $S_I/I^2 \sim 1/V$.[29,49] This leads to higher noise in QD films, which have fewer conducting channels. However, more experimental studies are required to establish the exact mechanism of the noise in such samples and discriminate the effect of differences in inter-QD distances and coupling, QD stoichiometry, surface doping, ligand coverage, and grain boundaries in QD films. We note that no theoretical models for low-frequency noise in QD films exist at the moment. The conventionally accepted noise models are either for electron band conduction in semiconductors[29,49] and metals[29,58,59] or electron hopping in disordered semiconductor systems.[43,60,61] Ordered and random-packed QD films are a unique class of materials that will require dedicated investigation. One should also note that

the signal-to-noise ratio of a photodetector system limited by $1/f$ noise cannot be improved by extending the measuring time, $t \propto 1/f$. The total accumulated energy of the flicker $1/f$ noise increases at least as fast as t. This consideration adds a practical motivation to more detail studies of low-frequency noise in colloidal QDs.

In conclusion, we reported on measurements of the low-frequency electronic noise in ordered (Langmuir-Schaefer), weakly-ordered (spin cast), and random-packed (dip coated) films of colloidal PbSe quantum dots. An important finding is that the normalized noise spectral density of the dark current contains a Lorentzian component superimposed on the $1/f$ background that is reminiscent of G–R noise. An activation energy of ~0.3 eV was extracted from the noise spectrum temperature dependence for both the ordered and random-packed films. The noise level in the ordered films was lower than that in the weakly-ordered and random-packed films. However, the measurements also reveal a large variation in noise levels between random-packed films prepared with different ligand treatments. The obtained results are important for application of colloidal quantum dot films in photodetectors.

Methods

Materials

All chemicals were used as received unless otherwise noted. Lead oxide (PbO, 99.999%), lead iodide (PbI$_2$, 99.9985%), and selenium shot (99.999%) were purchased from Alfa Aesar. Oleic acid (OA, technical grade, 90%), diphenylphosphine (DPP, 98%), 1-octadecene (ODE, 90%), anhydrous ethylene glycol (EG, 99.8%), anhydrous acetonitrile (99.99%), anhydrous hexanes (99%), anhydrous toluene (99.8%), 3-mercapto-propyltrimethoxysilane (3-MPTMS, 95%), trimethylaluminum (TMA, 97%), ammonium thiocyanate (NH$_4$SCN, 99.99%), and anhydrous dimethyl sulfoxide (DMSO, 99.9%) were purchased from Sigma Aldrich. Anhydrous 1,2-ethylenediamine (EDA, >98.0%) was purchased from TCI. Trioctylphosphine (TOP, technical grade, >90%) was acquired from Fluka and mixed with selenium shot for 24 hours to form a 1 M TOP-Se stock solution. 18.2 MΩ water (Milli-Q Gradient) was used for substrate cleaning and atomic layer deposition (ALD). Water for ALD was degassed with three freeze–pump–thaw cycles before use.

Quantum dot synthesis

PbSe QDs were synthesized and purified using standard air-free techniques. PbO (1.50 g), OA (5.00 g), and ODE (10.00 g) were mixed and degassed in a three-neck round-bottom flask at room temperature. Then the mixture was heated at 110 °C under vacuum to form Pb(OA)$_2$ and dry the solution. After 1.5 hours, the Pb(OA)$_2$ solution was heated to 180 °C under argon flow and 9.5 mL of a 1 M solution of TOP-Se containing 200 μL of DPP was rapidly injected into this hot solution. An immediate darkening of the solution was observed, and the QDs were grown for 105 seconds at ~160 °C. The reaction was quenched with a liquid nitrogen bath and injection of 10 mL

of anhydrous hexanes. The QDs were purified in an N_2-filled glovebox (<0.5 ppm O_2) by adding 15 mL of acetonitrile to the reaction solution, collecting the QDs by centrifugation, performing six cycles of redispersion/precipitation using toluene/acetonitrile (3 mL/22 mL), and then drying and storing the QDs as a powder in the glovebox.

Device fabrication

Pre-patterned Si/SiO$_2$ substrates were cleaned by 10 minute rounds of sonication in acetone, Millipore water, and isopropanol, then blown dry. Following cleaning, they were immersed in a 100 mM solution of 3-MPTMS in toluene for several hours, then rinsed with neat toluene and blown dry. Dip-coated films (DC films) were prepared by 10 sequential rounds of dipping pre-patterned substrates in: (1) a 4 g L^{-1} PbSe QD solution in hexanes for 1 second; (2) ligand exchange solution for 10 seconds; (3) a neat acetonitrile rinse for 3 seconds. For SCN films, a 15 mM NH$_4$SCN solution in acetonitrile was used. For EDA films, a 1 M EDA solution in acetonitrile was used. Spin-coated films (SC films) were prepared by spin-coating substrates with a 25 g L^{-1} PbSe QD solution in octane at a speed of 2000 rpm for 40 seconds. The films were then soaked in a fresh 105 mM EDA solution in ethylene glycol for ~1 minute, followed by a 5 minute soak in PbI$_2$ in DMSO, then rinsed clean in neat DMSO and acetonitrile. This process was repeated twice. LS films were prepared by self-assembly of 60 μL of 30 g L^{-1} PbSe QD solution suspended in hexanes on a liquid ethylene glycol (EG) surface in a Teflon well. After solution deposition, the well was covered and the hexanes allowed to evaporate over the course of ~25 minutes, leaving a dried QD superlattice film floating on the EG. The well was then uncovered and 100 μL of 7.5 M EDA in acetonitrile (105 mM EDA concentration overall in the well) was injected into the EG, underneath the edge of the film, to initiate ligand exchange. After ~30 seconds, the section of film nearest to the EDA injection point was manually stamp transferred to the pre-patterned Si/SiO$_2$ substrate using a vacuum wand. The stamped film was then rinsed in clean acetonitrile and blown dry with flowing N_2. Lastly, the film was soaked in a 10 mM PbI$_2$ in DMSO solution for 5 min before being rinsed in clean DMSO and acetonitrile, and again blown dry under flowing N_2. Atomic layer deposition was performed at 55 °C in homemade ALD system at a base pressure of 200 mTorr. ~20 nm thick films were produced after 200 cycles of alternating TMA and H$_2$O pulses. Dose times of 20 ms and wait times of 45 s were used for each precursor.

Conflicts of interest

There are no conflicts to declare.

Acknowledgements

References

1 D. V. Talapin, J. S. Lee, M. V. Kovalenko and E. V. Shevchenko, *Chem. Rev.*, 2010, **110**, 389–458.

2 J. P. Clifford, G. Konstantatos, K. W. Johnston, S. Hoogland, L. Levina and E. H. Sargent, *Nat. Nanotechnol.*, 2008, **4**, 40.

3 D. V. Talapin and C. B. Murray, *Science*, 2005, **310**, 86–89.

4 J. S. Lee, E. V. Shevchenko and D. V. Talapin, *J. Am. Chem. Soc.*, 2008, **130**, 9673–9675.

5 M. Law, J. M. Luther, Q. Song, B. K. Hughes, C. L. Perkins and A. J. Nozik, *J. Am. Chem. Soc.*, 2008, **130**, 5974–5985.

6 K. Rong, H. Liu, K. Shi and J. Chen, *Nanoscale*, 2019, **11**, 13885–13893.

7 J. Z. Fan, A. D. La Croix, Z. Yang, E. Howard, R. Quintero-Bermudez, L. Levina, N. M. Jenkinson, N. J. Spear, Y. Li, O. Ouellette, Z. H. Lu, E. H. Sargent and J. E. Macdonald, *Nanoscale*, 2019, **11**, 10774–10781.

8 Y. Zhou, H. Zhao, D. Ma and F. Rosei, *Chem. Soc. Rev.*, 2018, **47**, 5866–5890.

9 Y. Jiang, S. Y. Cho and M. Shim, *J. Mater. Chem. C*, 2018, **6**, 2618–2634.

10 R. Wang, Y. Shang, P. Kanjanaboos, W. Zhou, Z. Ning and E. H. Sargent, *Energy Environ. Sci.*, 2016, **9**, 1130–1143.

11 G. Konstantatos and E. H. Sargent, *Infrared Phys. Technol.*, 2011, **54**, 278–282.

12 Q. Shao, A. A. Balandin, A. I. Fedoseyev and M. Turowski, *Appl. Phys. Lett.*, 2007, **91**, 163503.

13 G. Konstantatos, I. Howard, A. Fischer, S. Hoogland, J. Clifford, E. Klem, L. Levina and E. H. Sargent, *Nature*, 2006, **442**, 180–183.

14 O. L. Lazarenkova and A. A. Balandin, *J. Appl. Phys.*, 2001, **89**, 5509–5515.

15 A. A. Balandin and O. L. Lazarenkova, *Appl. Phys. Lett.*, 2003, **82**, 415–417.

16 O. L. Lazarenkova and A. A. Balandin, *Phys. Rev. B: Condens. Matter Mater. Phys.*, 2002, **66**, 245319.

17 D. L. Nika, E. P. Pokatilov, Q. Shao and A. A. Balandin, *Phys. Rev. B: Condens. Matter Mater. Phys.*, 2007, **76**, 125417.

18 G. Springholz, V. Holy, M. Pinczolits and G. Bauer, *Science*, 1998, **282**, 734–737.

19 N. G. Stocks, *Phys. Rev. Lett.*, 2000, **84**, 2310–2313.

20 H. Z. Song, K. Akahane, S. Lan, H. Z. Xu, Y. Okada and M. Kawabe, *Phys. Rev. B: Condens. Matter Mater. Phys.*, 2001, **64**, 85303.

21 M. V. Artemyev, A. I. Bibik, L. I. Gurinovich, S. V. Gaponenko and U. Woggon, *Phys. Rev. B: Condens. Matter Mater. Phys.*, 1999, **60**, 1504–1506.

22 M. V. Artemyev, U. Woggon, H. Jaschinski, L. I. Gurinovich and S. V. Gaponenko, *J. Phys. Chem. B*, 2000, **104**, 11617–11621.

23 M. V. Artemyev, A. I. Bibik, L. I. Gurinovich, S. V. Gaponenko, H. Jaschinski and U. Woggon, *Phys. Status Solidi B*, 2001, **224**, 393–396.

24 S. Facsko, T. Dekorsy, C. Koerdt, C. Trappe, H. Kurz, A. Vogt and H. L. Hartnagel, *Science*, 1999, **285**, 1551–1553.

25 R. A. Rupani, S. Ghosh, X. Su and P. Bhattacharya, *Microelectron. J.*, 2008, **39**, 307–313.

26 D. Lachance-Quirion, S. Tremblay, S. A. Lamarre, V. Méthot, D. Gingras, J. Camirand Lemyre, M. Pioro-Ladrière and C. N. Allen, *Nano Lett.*, 2014, **14**, 882–887.

27 H. Liu, E. Lhuillier and P. Guyot-Sionnest, *J. Appl. Phys.*, 2014, **115**, 154309.

28 L. Colace, A. De Iacovo and C. Venettacci, *Phys. Status Solidi C*, 2017, **14**, 1700185.

29 A. A. Balandin, *Noise and Fluctuations Control in Electronic Devices*, World Scientific Publishing Co., 2003, vol. 03.

30 R. Pettai, *Noise in Receiving Systems*, Wiley, New York, 1984.

31 F. C. Motchenbacher and C. D. Fitchen, *Low-Noise Electronic System Design*, Wiley, New York, 1973.

32 R. A. Potyrailo, C. Surman, N. Nagraj and A. Burns, *Chem. Rev.*, 2011, **111**, 7315–7354.

33 A. A. Balandin, *Nat. Nanotechnol.*, 2013, **8**, 549.

34 E. J. McDowell, J. Ren and C. Yang, *Opt. Express*, 2008, **16**, 6822–6832.

35 Y. Liu, M. Gibbs, C. L. Perkins, J. Tolentino, M. H. Zarghami, J. Bustamante and M. Law, *Nano Lett.*, 2011, **11**, 5349–5355.

36 A. Dong, Y. Jiao and D. J. Milliron, *ACS Nano*, 2013, **7**, 10978–10984.

37 K. Whitham, J. Yang, B. H. Savitzky, L. F. Kourkoutis, F. Wise and T. Hanrath, *Nat. Mater.*, 2016, **15**, 557.

38 M. Abelson, A. Qian, C. Salk, T. Luan, Z. Fu, K. Zheng, J. G. Wardini and J. L. Law, *Nat. Mater.*, 2019, DOI: 10.1038/s41563-019-0485-2.

39 J. M. Luther, M. Law, M. C. Beard, Q. Song, M. O. Reese, R. J. Ellingson and A. J. Nozik, *Nano Lett.*, 2008, **8**, 3488–3492.

40 W. H. Strehlow and E. L. Cook, *J. Phys. Chem. Ref. Data*, 1973, **2**, 163–200.

41 Y. Liu, M. Gibbs, J. Puthussery, S. Gaik, R. Ihly, H. W. Hillhouse and M. Law, *Nano Lett.*, 2010, **10**, 1960–1969.

42 B. I. Shklovskiĭ and A. L. Éfros, *Sov. Phys. Uspekhi*, 1975, **18**, 845–862.

43 B. I. Shklovskii, *Solid State Commun.*, 1980, **33**, 273–276.

44 V. C. Lopes, A. J. Syllaios, D. Whitfield, K. Shrestha and C. L. Littler, *MRS Proc.*, 2015, **1770**, 25–30.

45 P. Guyot-Sionnest, *J. Phys. Chem. Lett.*, 2012, **3**, 1169–1175.

46 A. K. Geremew, F. Kargar, E. X. Zhang, S. E. Zhao, E. Aytan, M. A. Bloodgood, T. T. Salguero, S. Rumyantsev, A. Fedoseyev, D. M. Fleetwood and A. A. Balandin, *Nanoscale*, 2019, **11**, 8380–8386.

47 M. Zahid Hossain, S. Rumyantsev, M. S. Shur and A. A. Balandin, *Appl. Phys. Lett.*, 2013, **102**, 153512.

48 G. Liu, S. Rumyantsev, M. A. Bloodgood, T. T. Salguero and A. A. Balandin, *Nano Lett.*, 2018, **18**, 3630–3636.

49 P. Dutta and P. M. Horn, *Rev. Mod. Phys.*, 1981, **53**, 497.

50 V. Mitin, L. Reggiani and L. Varani, *Noise Fluctuations Control Electron. Devices*, ed. A. A. Balandin, World Scientific Publishing Co., 2nd edn, 2003, vol. 3, pp. 1–19.

51 M. J. Kirton and M. J. Uren, *Adv. Phys.*, 1989, **38**, 367.

52 Z. Çelik-Butler, P. Vasina and N. V. Amarasinghe, *IEEE Trans. Electron Devices*, 2000, **47**, 646.

53 M. E. Levinshtein and S. L. Rumyantsev, *Semicond. Sci. Technol.*, 1994, **9**, 1183.

54 A. K. Geremew, S. Rumyantsev, M. A. Bloodgood, T. T. Salguero and A. A. Balandin, *Nanoscale*, 2018, **10**, 19749–19756.

55 Z. Celik-Butler and T. Y. Hsiang, *Solid-State Electron.*, 1987, **30**, 419–423.

56 S. Christensson, I. Lundström and C. Svensson, *Solid-State Electron.*, 1968, **11**, 797–812.

57 D. M. Fleetwood, *IEEE Trans. Nucl. Sci.*, 2015, **62**, 1462–1486.

58 V. Galperin, Yu. M. Karpov and V. G. Kozub, *Sov. Phys. JETP*, 1989, **68**, 648–653.

59 A. P. Dmitriev, M. E. Levinshtein and S. L. Rumyantsev, *J. Appl. Phys.*, 2009, **106**, 24514.

60 B. I. Shklovskii, *Phys. Rev. B: Condens. Matter Mater. Phys.*, 2003, **67**, 45201.

61 A. L. Burin, B. I. Shklovskii, V. I. Kozub, Y. M. Galperin and V. Vinokur, *Phys. Rev. B: Condens. Matter Mater. Phys.*, 2006, **74**, 75205.